Role of wall deformability on interfacial instabilities in gravity-driven two-layer flow with a free surface

Gaurav and V. Shankar[a)]
Department of Chemical Engineering, Indian Institute of Technology, Kanpur 208 016, India

(Received 19 December 2009; accepted 28 July 2010; published online 15 September 2010)

The linear stability of gravity-driven flow of two superposed Newtonian liquid layers down a deformable, inclined, wall is analyzed in order to examine the effect of wall deformability on the interfacial instabilities in the system. There are three distinct interfacial modes in this composite system, viz., gas-liquid (GL), liquid-liquid (LL), and liquid-solid (LS) modes. For a rigid-wall, the GL interface becomes unstable above a critical Reynolds number, while the stability of the LL interface depends on the relative placement of the liquid layers. When the more viscous liquid is adjacent to rigid surface, the LL mode becomes unstable beyond a critical Reynolds number (Re), while it becomes unstable even at Re=0 when the less viscous liquid is next to rigid-wall. Our asymptotic results show that solid deformability has a stabilizing effect on both GL and LL modes in the low-wavenumber limit when the more viscous liquid layer is near the deformable wall. Numerical results reveal that both the GL and LL interfacial instabilities can be suppressed for all wavenumbers when the solid layer becomes sufficiently deformable. With further increase in solid deformability, all three interfacial modes become unstable. However, the parameters characterizing the solid (shear modulus, thickness, and solid viscosity) can be chosen such that the GL and LL interfaces remain stable (which are otherwise unstable in flow down a rigid incline) at all wavenumbers without the destabilization of LS interface. When the thickness of the top (less viscous) liquid layer is greater, it is more difficult to obtain stable flow configuration by manipulating the solid parameters. When the less viscous liquid is adjacent to the deformable surface, solid deformability always has a destabilizing effect on LL interfacial mode, and it is not possible to simultaneously stabilize both GL and LL interfaces for this configuration. © *2010 American Institute of Physics*. [doi:10.1063/1.3480633]

I. INTRODUCTION

The flow of two or more immiscible liquid layers is encountered in a variety of settings including coextrusion of polymers,[1–5] coating processes,[6] as well as in microfluidic devices[7] designed for the production of monodisperse emulsions. Multilayer flows are susceptible to instabilities at the interface between the liquid layers or at the interface between the liquid and gas (i.e., free surface). Such instabilities are detrimental to product quality in coating processes where uniform film thickness is of importance.[6] On the other hand, these instabilities may be exploited to increase rates of transport or in the creation of drops and particles in microfluidic devices which involve flow of two or more liquids. A key feature in multilayer flows is the ability to manipulate (induce or suppress) interfacial instabilities occurring at the multiple interfaces. In this study, we evaluate the feasibility of using a "passive" deformable solid coating to suppress or enhance the free-surface and liquid-liquid interfacial instabilities, by considering gravity-driven two-layer flow of two Newtonian liquids with a free surface. The results of the present study could be potentially relevant to microfluidic devices used in the preparation of micron-sized drops and particles,[7] where the ability to control the interfacial instability between the two fluids determines the size of the drops formed. Since microfluidic devices are often fabricated using polydimethyl siloxane based elastomers, the present study suggests the strategy of tailoring the modulus of the elastomer to achieve control over the interfacial instabilities. Below, we briefly review the relevant literature on this subject and motivate the context and importance of the present study.

Benjamin[8] and Yih[9] employed a long-wave asymptotic analysis and showed that (Newtonian) liquid flow down an inclined plane could become unstable above a critical Reynolds number, which is zero for a vertically inclined plane. Lin[10] extended the results to disturbances of arbitrary wavelengths and demonstrated that long-wave disturbances are the dominant mode of instability. The presence of another liquid layer in the case of two-layer flow down an inclined plane renders the flow unstable[11–15] even at zero Reynolds number when the less viscous fluid is adjacent to the inclined wall. This instability arises due to the interaction between free-surface and the liquid-liquid interfaces. Inertia has a stabilizing effect on the liquid-liquid (LL) mode for long-waves and destabilizing effect for finite and short-waves. However, inertia is always destabilizing for the gas-liquid (GL) mode, and the GL interface becomes unstable above a critical Reynolds number. The LL interfacial mode can be completely stabilized at sufficiently high Reynolds number, when the interfacial tension increases beyond a critical value, but the

a)Author to whom correspondence should be addressed. Electronic mail: vshankar@iitk.ac.in.

GL mode becomes unstable. Thus, simultaneous stabilization of both free-surface and LL interfacial modes is not possible when the less viscous liquid is adjacent to the rigid-wall. When the more viscous liquid is placed near the rigid inclined wall, the system is stable at zero Reynolds number and inertia is destabilizing for both LL and GL interfacial modes. Both GL and LL interfaces become unstable above a critical Reynolds number and this critical Reynolds number is zero for a rigid vertical plane.

While the above studies have employed the classical temporal stability analysis, there has also been a lot of attention on the spatiotemporal formulation to capture the convective nature of the unstable modes.[16–18] The spatiotemporal approach to stability[19] provides a more clearer picture of the instability by distinguishing it as being either convective or absolute. In this study, however, we are mainly interested in obtaining neutral stability curves (in appropriate parameter space) which depict parameter regimes where the interfacial instabilities are fully suppressed. Neutral curves remain the same regardless of whether the modes considered are temporal or spatial because the growth rate is by definition zero along the neutral curve. Hence, we restrict ourselves to the classical temporal analysis to obtain the neutral curves. There have also been many studies[20,21] which have studied the nonlinear regime by using (lubricationlike) long-wave theories to derive the evolution equation for the interfacial deformations. As discussed in detail below, in the present system, even finite-wavenumber modes can be the most unstable when the wall is deformable, and restriction to purely long-waves does not yield the complete picture of the system's stability.

Previous studies have also explored the possibility of controlling the interfacial instability in multilayer flows by various methodologies. Lin *et al.*[22–24] studied the effect of in-plane horizontal oscillations on the free-surface instability in single and two-layer flows using Floquet theory. They showed that the onset of instability in this system can be suppressed in certain parameter regimes by imparting oscillations of appropriate amplitude and frequencies. They also demonstrated that outside these windows of stability, it is possible to even enhance the instability of liquid film. The possibility of using deformable solid layer coating to manipulate and suppress interfacial instabilities has been explored for two-layer plane Couette flow[25,26] and single-layer free-surface flow[27–29] of both Newtonian and viscoelastic liquids. It was shown[25,27] that the deformability of the solid could lead to complete suppression of the interfacial instabilities. Gkanis and Kumar[30] analyzed the stability of gravity-driven flow past a deformable neo-Hookean solid in the creeping-flow limit (Re=0) and pointed out the importance of using a nonlinear constitutive model for the solid. While many previous studies (including our earlier works, e.g., Refs. 26 and 27) considered a simple linearized elastic (i.e., Hookean) model for the deformable solid, it is, however, not valid for large deformations encountered in soft solids. Although we are interested here only in linear stability (wherein the fluctuations are deemed infinitesimal), the base-state of the solid has $O(1)$ deformations. The crucial coupling between the $O(1)$ base-state and fluctuations was neglected in the earlier works, and this leads to qualitatively different predictions. Importantly, all these prior studies were restricted to the case where the deformability of the solid layer stabilized only one unstable interface, which could be a liquid-liquid interface (Refs. 25 and 26) or a gas-liquid free surface (Refs. 27–30).

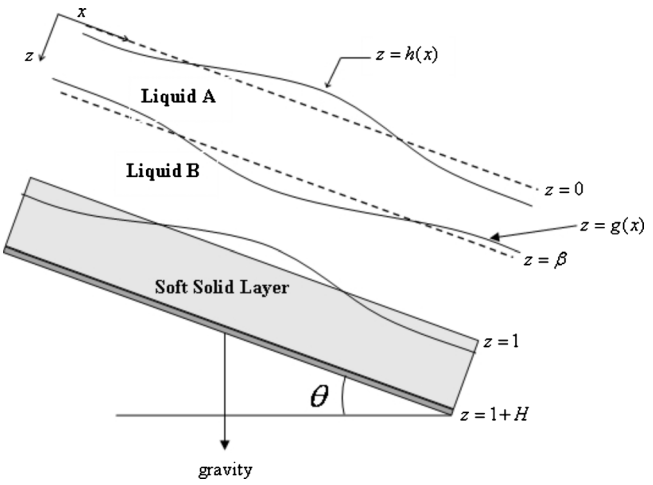

FIG. 1. Schematic diagram showing the configuration and (nondimensional) coordinate system considered in this work: two Newtonian liquid films flowing past an inclined plane lined with a viscoelastic neo-Hookean solid layer.

In this work, we focus on the question of whether the presence of a deformable solid can simultaneously stabilize two unstable interfaces (viz., a liquid-liquid interface and a gas-liquid interface). We also explore the parametric regimes where the instability can be enhanced by manipulating the properties of soft solid coating. There have been many studies (Refs. 2 and 3, for example) which have analyzed the stability of two- and three-layer flows of polymeric (viscoelastic) fluids encountered in coextrusion operations. It is nevertheless instructive to analyze the stability of two Newtonian liquid layers for the following reason: it has been shown using asymptotic analysis and numerical solutions that[26,29] that the (qualitative) effect of deformable layer on the interfacial mode(s) is independent of whether the fluids are Newtonian or viscoelastic. Hence, many of the qualitative features of the present results are expected to carry over to the case when both the fluids are viscoelastic. The rest of this paper is structured as follows: after formulating the problem in Sec. II, we discuss results from the low-wavenumber asymptotic analysis in Sec. III A. Results from the numerical solution for arbitrary wavenumbers are discussed in Sec. III C, and the salient conclusions of this work are summarized in Sec. IV.

II. PROBLEM FORMULATION

A. Governing equations for fluid and solid

We consider the gravity-driven laminar flow of two superposed Newtonian liquids flowing past an incompressible and impermeable deformable solid (Fig. 1). The solid (of thickness HR, shear modulus E, and viscosity η_s) is strongly

bonded to a rigid inclined plane at $z^*=(1+H)R$ which makes an angle θ with the horizontal. The top layer (liquid A of viscosity μ_a) is in contact with a passive gas and occupies a region $0\leq z^*\leq \beta R$ in the unperturbed base-state. The bottom layer (liquid B of viscosity μ_b) is adjacent to the deformable solid layer and occupies a region $\beta R\leq z^*\leq R$ in the unperturbed base-state. The densities (ρ) of two liquid layers are assumed to be equal to the density of solid because the densities of commonly used polymeric materials are, in general, not very different from those of common liquids. Various physical quantities are nondimensionalized by using the following scales: R for lengths and displacements, $V=\rho g R^2 \sin\theta/2\mu_b$ for velocities, and $\mu_b V/R$ for stresses and pressure. The governing equations for the two liquid layers are Navier–Stokes continuity and momentum equations,

$$\nabla\cdot\mathbf{v}^\alpha=0,$$
$$\mathrm{Re}[\partial_t\mathbf{v}^\alpha+\mathbf{v}^\alpha\cdot\nabla\mathbf{v}^\alpha]=-\nabla p^\alpha+\mu_{\mathrm{r}}^\alpha\nabla\cdot\mathbf{T}^\alpha+\frac{2}{\sin\theta}\hat{\mathbf{g}}, \tag{1}$$

where $\mathbf{v}^\alpha$ and p^α are the velocity and pressure fields in liquid layer $\alpha=a,b$; $\mu_{\mathrm{r}}^\alpha=\mu_{\mathrm{r}}=\mu_a/\mu_b$ for liquid A ($\alpha=a$) and $\mu_{\mathrm{r}}^\alpha=1$ for liquid B ($\alpha=b$); $\mathbf{T}^\alpha=-p^\alpha\mathbf{I}+\mu_{\mathrm{r}}^\alpha[\nabla\mathbf{v}^\alpha+(\nabla\mathbf{v}^\alpha)^T]$ is the total stress tensor for liquid layer α ($=a$ or b), and $\mathrm{Re}=\rho VR/\mu_b$ is the Reynolds number based on the viscosity of fluid B.

The governing equations for the liquid layers are written in terms of spatial (Eulerian) coordinates ($\mathbf{x}=x,y,z$). It is possible to express the dynamical quantities and governing equations in the solid also in a consistent Eulerian fashion.[39,46] Equivalently, following Ref. 31, we find it convenient to refer the governing equations for the solid in terms of a reference (Lagrangian) configuration, where the independent variables are the positions $\mathbf{X}=(X,Y,Z)$ of material particles in the reference (i.e., unstressed solid) configuration. Chokshi[39] has shown that the Eulerian–Eulerian and Eulerian–Lagrangian approaches are equivalent and yield the same result for the eigenvalues. Thus, the spatial coordinates (x,y,z) used for fluid motion is identical to the reference coordinates (X,Y,Z) in the unstressed configuration for the deformable solid. In the deformed state of the solid, the spatial positions of the material particles are denoted in this study by $\mathbf{w}(\mathbf{X})$, where $\mathbf{w}=(w_X,w_Y,w_Z)$, while $\mathbf{X}=(X,Y,Z)$ denotes the position vector of the material particle in the reference configuration. The deformable solid layer is modeled as an incompressible neo-Hookean viscoelastic solid and the mass and momentum conservation equations governing the dynamics of solid are given as[32,33]

$$\det(\mathbf{F})=1,\quad \mathrm{Re}\left[\frac{\partial^2\mathbf{w}}{\partial t^2}\right]_{\mathbf{X}}=\nabla_{\mathbf{X}}\cdot\mathbf{P}+\frac{2}{\sin\theta}\hat{\mathbf{g}}. \tag{2}$$

In the above equations, $\mathbf{F}$ is the deformation gradient tensor defined as $\mathbf{F}=\nabla_{\mathbf{X}}\mathbf{w}$ and $\mathbf{P}$ is the first Piola–Kirchhoff stress tensor. The first Piola–Kirchhoff stress tensor is related to Cauchy stress tensor by $\mathbf{P}=\mathbf{F}^{-1}\cdot\boldsymbol{\sigma}$. The Cauchy stress tensor $\boldsymbol{\sigma}$ for the neo-Hookean viscoelastic solid is split into an elastic part, $\boldsymbol{\sigma}_e$, and a dissipative part, $\boldsymbol{\sigma}_d$ (Refs. 34–37) $\boldsymbol{\sigma}=\boldsymbol{\sigma}_e+\boldsymbol{\sigma}_d$,

$$\boldsymbol{\sigma}_e=-\hat{p}_s\mathbf{I}+\frac{1}{\Gamma}(\mathbf{F}\cdot\mathbf{F}^{\mathbf{T}}),\quad \boldsymbol{\sigma}_{\mathbf{d}}=\eta_{\mathbf{r}}(\mathbf{L}+\mathbf{L}^{\mathbf{T}}), \tag{3}$$

where $\Gamma=\mu_b V/ER$ is the nondimensional solid deformability parameter. When $\Gamma\to 0$, we obtain the limit of a rigid solid layer; $\hat{p}_s$ is the pressurelike function related to actual pressure in the neo-Hookean solid as $\hat{p}_s=p_s+1/\Gamma$; $\mathbf{L}=\dot{\mathbf{F}}\cdot\mathbf{F}^{-1}$ is the spatial velocity gradient and $\eta_r=\eta_s/\mu_b$ is the ratio of solid to liquid B viscosity. To simplify our calculations, we assume a frequency-independent viscosity to describe the dissipative effects in solid medium. The conditions at the GL interface are kinematic condition for the evolution of the free surface and tangential and normal stress balances. The tangential stresses at the free surface are zero and normal stress in the liquid A is balanced by the hydrostatic pressure in the gas adjacent to it. At the LL and LS interfaces, the relevant conditions are those of continuity of velocities and stresses. At $z=1+H$, the deformable solid is strongly bonded to a rigid surface and hence the boundary conditions are those of no deformations.

In the base-state, the GL, LL, and LS interfaces remain flat and unperturbed, and there is a steady unidirectional flow in the two liquid layers in the x-direction. The solid is at rest with a nonzero displacement in x-direction due to shear stress exerted by liquid B at the LS interface. The nondimensional velocity profile and pressure distribution in the two liquid layers are given as

$$\bar{v}_x^a(z)=\left[1+\beta^2(1/\mu_r-1)-\frac{z^2}{\mu_{\mathrm{r}}}\right],\quad \bar{p}^a(z)=(2\cot\theta)z, \tag{4}$$

$$\bar{v}_x^b(z)=(1-z^2),\quad \bar{p}^b(z)=(2\cot\theta)z, \tag{5}$$

where $\mu_{\mathrm{r}}=\mu_a/\mu_b$ is the viscosity ratio, β is the mean position of the LL interface (see Fig. 1), and the overbar is used to denote various base-state physical quantities. The deformation and pressure fields for solid layer are given by

$$\bar{w}_X=X+\Gamma[(1+H)^2-Z^2],$$
$$\bar{w}_Z=Z,\quad \bar{\hat{p}}_s=\frac{1}{\Gamma}+(2\cot\theta)Z. \tag{6}$$

B. Linearized governing equations and interface conditions

A standard temporal linear stability analysis is performed in order to determine the stability of the present three-layered configuration. The perturbations are considered to be two-dimensional (in the x and z directions), which are expanded in the form of Fourier modes, $f'=\tilde{f}(z)\exp[ik(x-ct)]$, where f' is the perturbation to any physical variable, k is the (real) wavenumber of perturbations, c is the complex wave-speed, and $\tilde{f}(z)$ is the complex amplitude function of the disturbance. For the deformable solid, x and z are replaced by X and Z, respectively. If $c_i>0$ (or $c_i<0$), flow will be unstable (or stable). The linearized stability equations for liquid layer $\alpha(=a,b)$ are

$$\frac{\mathrm{d}\tilde{v}_z^{\alpha}}{\mathrm{d}z} + \mathrm{i}k\tilde{v}_x^{\alpha} = 0, \tag{7}$$

$$\mathrm{Re}[\mathrm{i}k(\bar{v}_x^{\alpha} - c)\tilde{v}_x^{\alpha} + (\mathrm{d}_z\bar{v}_x^{\alpha})\tilde{v}_z^{\alpha}] = -\mathrm{i}k\tilde{p}^{\alpha} + \mu_{\mathrm{r}}^{\alpha}\left[\frac{\mathrm{d}^2}{\mathrm{d}z^2} - k^2\right]\tilde{v}_x^{\alpha}, \tag{8}$$

$$\mathrm{Re}[\mathrm{i}k(\bar{v}_x^{\alpha} - c)\tilde{v}_z^{\alpha}] = -\frac{\mathrm{d}\tilde{p}^{\alpha}}{\mathrm{d}z} + \mu_{\mathrm{r}}^{\alpha}\left[\frac{\mathrm{d}^2}{\mathrm{d}z^2} - k^2\right]\tilde{v}_z^{\alpha}. \tag{9}$$

The linearized equations for the neo-Hookean viscoelastic solid are

$$\frac{\mathrm{d}\tilde{w}_Z}{\mathrm{d}Z} + \mathrm{i}k\tilde{w}_X - \left(\frac{\mathrm{d}\bar{w}_X}{\mathrm{d}Z}\right)\mathrm{i}k\tilde{w}_Z = 0, \tag{10}$$

$$\begin{aligned}
&-\mathrm{i}k\tilde{p}_s + (2\cot\theta)\mathrm{i}k\tilde{w}_Z + \frac{1}{\Gamma}\left[-k^2 + \frac{\mathrm{d}^2}{\mathrm{d}Z^2}\right]\tilde{w}_X - \mathrm{i}kc\,\eta_r \\
&\quad\times\left[-2k^2\tilde{w}_X + \frac{\mathrm{d}^2\tilde{w}_X}{\mathrm{d}Z^2} - \left(\frac{\mathrm{d}\bar{w}_X}{\mathrm{d}Z}\right)\left(-k^2\tilde{w}_Z + 2\mathrm{i}k\frac{\mathrm{d}\tilde{w}_X}{\mathrm{d}Z}\right)\right] \\
&\quad-\mathrm{i}kc\,\eta_r\left[\mathrm{i}k\frac{\mathrm{d}\tilde{w}_Z}{\mathrm{d}Z} - \left(\frac{\mathrm{d}\bar{w}_X}{\mathrm{d}Z}\right)^2 k^2\tilde{w}_X - \left(\frac{\mathrm{d}^2\bar{w}_X}{\mathrm{d}Z^2}\right)\mathrm{i}k\tilde{w}_X\right] \\
&\quad= -k^2c^2\,\mathrm{Re}\,\tilde{w}_X,
\end{aligned} \tag{11}$$

$$\begin{aligned}
&\left(\frac{\mathrm{d}\bar{w}_X}{\mathrm{d}Z}\right)\mathrm{i}k\tilde{p}_s - (2\cot\theta)\mathrm{i}k\tilde{w}_X - \frac{\mathrm{d}\tilde{p}_s}{\mathrm{d}Z} + \frac{1}{\Gamma}\left[-k^2 + \frac{\mathrm{d}^2}{\mathrm{d}Z^2}\right]\tilde{w}_Z \\
&\quad-\mathrm{i}kc\,\eta_r\left[-\left(\frac{\mathrm{d}\bar{w}_X}{\mathrm{d}Z}\right)\left(-k^2\tilde{w}_X + 4\mathrm{i}k\frac{\mathrm{d}\tilde{w}_Z}{\mathrm{d}Z}\right)\right. \\
&\quad\left.-2\left(\frac{\mathrm{d}\bar{w}_X}{\mathrm{d}Z}\right)^2 k^2\tilde{w}_Z\right] - \mathrm{i}kc\,\eta_r\left[-2\mathrm{i}k\left(\frac{\mathrm{d}^2\bar{w}_X}{\mathrm{d}Z^2}\right)\tilde{w}_Z\right. \\
&\quad\left.+\mathrm{i}k\frac{\mathrm{d}\tilde{w}_X}{\mathrm{d}Z} + 2\frac{\mathrm{d}^2\tilde{w}_Z}{\mathrm{d}Z^2} - k^2\tilde{w}_Z\right] = -k^2c^2\,\mathrm{Re}\,\tilde{w}_Z.
\end{aligned} \tag{12}$$

The interface conditions at the known unperturbed GL interface position ($z=0$) are obtained by Taylor-expanding (and linearizing) the fluid dynamical variables about the flat interface in the base-state,

$$\mathrm{i}k[\bar{v}_x^a(z=0) - c]\tilde{h} = \tilde{v}_z^a(z=0), \tag{13}$$

$$-2\tilde{h} + \mu_{\mathrm{r}}\left(\frac{\mathrm{d}\tilde{v}_x^a}{\mathrm{d}z} + \mathrm{i}k\tilde{v}_z^a\right) = 0, \tag{14}$$

$$-\tilde{p}^a - (2\cot\theta)\tilde{h} + 2\mu_{\mathrm{r}}\frac{\mathrm{d}\tilde{v}_z^a}{\mathrm{d}z} - k^2\Sigma\tilde{h} = 0, \tag{15}$$

where $\Sigma = \gamma/\mu_b V$ is the nondimensional interfacial tension of the GL interface, with γ being the dimensional GL interfacial tension. Similarly, the linearized kinematic and interfacial conditions at the unperturbed LL interface ($z=\beta$) are given by

$$\mathrm{i}k[\bar{v}_x^a(z=\beta) - c]\tilde{g} = \tilde{v}_z^a(z=\beta), \tag{16}$$

$$\tilde{v}_x^a + \tilde{g}(\mathrm{d}_z\bar{v}_x^a)_{z=\beta} = \tilde{v}_x^b + \tilde{g}(\mathrm{d}_z\bar{v}_x^b)_{z=\beta}, \tag{17}$$

$$\mu_{\mathrm{r}}(\mathrm{d}_z\tilde{v}_x^a + \mathrm{i}k\tilde{v}_z^a) = (\mathrm{d}_z\tilde{v}_x^b + \mathrm{i}k\tilde{v}_z^b), \tag{18}$$

$$-\tilde{p^a} + 2\mu_{\mathrm{r}}\mathrm{d}_z\tilde{v}_z^a + \Sigma_1 k^2\tilde{g} = -\tilde{p^b} + 2\mathrm{d}_z\tilde{v}_z^b, \tag{19}$$

where $\Sigma_1 = \gamma_1/\mu_b V$ is the nondimensional liquid-liquid interfacial tension, with γ_1 being the dimensional LL interfacial tension. While the Eulerian description is used for both liquid layers, a Lagrangian framework is used here for the solid layer. Thus, the treatment of interfacial conditions at perturbed LS interface is different compared to conditions at GL or LL interface and is discussed in detail in Ref. 38. As explained there, a Taylor series expansion is not required to evaluate any solid variable on perturbed interface in the Lagrangian description of solid.[39] Following the procedure outlined in Ref. 38, the linearized conditions at LS interface are

$$\tilde{v}_z^b = -\mathrm{i}kc\tilde{w}_Z, \tag{20}$$

$$\tilde{v}_x^b + \tilde{w}_Z(\mathrm{d}_z\bar{v}_x^b)_{z=1} = -\mathrm{i}kc\tilde{w}_X, \tag{21}$$

$$\begin{aligned}
&\frac{1}{\Gamma}\left(\frac{\mathrm{d}\bar{w}_X}{\mathrm{d}Z}\right)\frac{\mathrm{d}\tilde{w}_Z}{\mathrm{d}Z} + \left(\frac{1}{\Gamma} - \mathrm{i}kc\,\eta_r\right)\left(\frac{\mathrm{d}\tilde{w}_X}{\mathrm{d}Z} + \mathrm{i}k\tilde{w}_Z\right) \\
&\quad-\frac{1}{\Gamma}\left(\frac{\mathrm{d}\bar{w}_X}{\mathrm{d}Z}\right)^2\mathrm{i}k\tilde{w}_Z - k^2c\,\eta_r\left(\frac{\mathrm{d}\bar{w}_X}{\mathrm{d}Z}\right)\tilde{w}_X \\
&\quad= \left(\frac{\mathrm{d}\tilde{v}_x^b}{\mathrm{d}z} + \mathrm{i}k\tilde{v}_z^b\right) + \tilde{w}_Z(\mathrm{d}_z^2\bar{v}_x^b),
\end{aligned} \tag{22}$$

$$\begin{aligned}
&-\tilde{p}_s + 2\left(\frac{1}{\Gamma} - \mathrm{i}kc\,\eta_r\right)\frac{\mathrm{d}\tilde{w}_Z}{\mathrm{d}Z} + \tilde{w}_Z\frac{\mathrm{d}\bar{p}^b}{\mathrm{d}z} - 2k^2c\,\eta_r\left(\frac{\mathrm{d}\bar{w}_X}{\mathrm{d}Z}\right)\tilde{w}_Z \\
&\quad= -\tilde{p^b} + 2\frac{\mathrm{d}\tilde{v}_z^b}{\mathrm{d}z} + k^2\Sigma_2\tilde{w}_Z,
\end{aligned} \tag{23}$$

where $\Sigma_2 = \gamma_2/\mu_b V$ is the nondimensional liquid-solid interfacial tension, with γ_2 being the dimensional LS interfacial tension. Finally, zero-displacement boundary conditions hold at the rigid surface ($z=1+H$) are $\tilde{w}_Z=0$, $\tilde{w}_X=0$.

III. RESULTS

A. Long-wave asymptotic analysis

We summarize here the salient results from a long-wave asymptotic analysis in order to elucidate the effect of a third solid layer on the stability of gravity-driven flow of two liquid layers down an inclined plane. We present only the results here, and the details of procedure can be found in earlier works[25,27] where the deformable solid layer was modeled as a linear viscoelastic solid. For $k \ll 1$, the complex wave-speed is expanded in an asymptotic series in k: $c = c^{(0)} + kc^{(1)} + \cdots$. The two roots for $c^{(0)}$ (corresponding to GL and LL interfaces) are found to be real and the system is neutrally stable at leading order; the roots are in exact agreement with the two leading order wave-speeds found by Kao[11] for a rigid inclined plane. Thus, the presence of deformable solid layer

does not affect the wave-speeds at the leading order. The root that approaches the single-layer free surface wave-speed,[9] when the two liquid layers are reduced to a single liquid layer, corresponds to the free surface or GL mode $c_{gl}^{(0)}$. The other root corresponds to the LL interfacial mode $c_{ll}^{(0)}$. Because the system is neutrally stable at leading order, it is necessary to solve for the first correction to wave-speed in order to determine the stability of the system.

When μ_r and β are numerically specified, it is possible to obtain an analytical expression for $c^{(1)}$. We first consider the case when the more viscous liquid is adjacent to the soft solid layer ($\mu_r<1$). As a representative example of results in the limit of low-wavenumbers, we consider $\mu_r=0.5$ and $\beta=0.5$; the leading order and first correction to wave-speed for both GL and LL modes are given by

$$c_{gl}^{(0)} = 2.425\ 39, \tag{24}$$

$$c_{gl}^{(1)} = \mathrm{i}[0.904(\mathrm{Re}) - 0.720(\cot\theta) - 4.319(\Gamma H)], \tag{25}$$

$$c_{ll}^{(0)} = 0.824\ 609, \tag{26}$$

$$c_{ll}^{(1)} = \mathrm{i}[3.86\times10^{-3}(\mathrm{Re}) - 3.011\times10^{-2} \times(\cot\theta) - 1.807\times10^{-1}(\Gamma H)]. \tag{27}$$

The leading order wave-speeds are identical to the results of Ref. 11 obtained for a rigid incline. However, the first correction is purely imaginary and has three contributions. For both GL and LL modes, the first term proportional to Re is destabilizing and the second term proportional to cot θ is stabilizing. These two contributions are exactly identical to the long-wave results obtained for a rigid incline.[11] The third term, proportional to ΓH in $c_{gl}^{(1)}$ and $c_{ll}^{(1)}$, represents the effect of solid layer deformability on the GL and LL modes, respectively. This term occurs with a negative sign implying that the deformable solid layer has stabilizing effect on both the modes. For $\Gamma\to0$ (the limit of rigid solid) or $H=0$ (the absence of deformable solid), each interfacial mode can become unstable above a critical Re and for $\theta=\pi/2$, both interfaces are unstable at any nonzero Reynolds number. For appropriately chosen nonzero values of ΓH, it is possible to suppress the low-wavenumber GL and LL mode instabilities. The above results [Eqs. (24)–(27)] are for $\mu_r=0.5$, $\beta=0.5$. We have verified that the qualitative nature of each term in $c_{gl}^{(1)}$ and $c_{ll}^{(1)}$ is independent of β and $\mu_r<1$. This is illustrated in Tables I and II in the Appendix, which summarize the results for $\mu_r=0.5$ and different values of β for GL and LL modes.

We next consider the case when less viscous liquid is adjacent to the deformable solid layer ($\mu_r>1$). For example, when $\mu_r=2$ and $\beta=0.5$, the leading order and first correction to wave-speed for both the modes are

$$c_{gl}^{(0)} = 1.809\ 02, \tag{28}$$

$$c_{gl}^{(1)} = \mathrm{i}[0.406(\mathrm{Re}) - 0.638(\cot\theta) - 3.831(\Gamma H)], \tag{29}$$

$$c_{ll}^{(0)} = 0.690\ 983, \tag{30}$$

$$c_{ll}^{(1)} = \mathrm{i}[-1.20\times10^{-3}(\mathrm{Re}) + 1.36\times10^{-2} \times(\cot\theta) + 8.156\times10^{-2}(\Gamma H)]. \tag{31}$$

The qualitative nature of different contributions in the expression of $c_{gl}^{(1)}$ remains same as in the case of $\mu_r<1$: the term proportional to Re is destabilizing, the term proportional to cot θ is stabilizing, and the soft solid contribution is stabilizing. Therefore, for a given H, it is still possible to stabilize the GL interface when Γ increases above a critical value. On the other hand, the nature of contributions of different terms in $c_{ll}^{(1)}$ changes when compared to the case when $\mu_r<1$. The contributions already present in a rigid surface have opposite behavior, i.e., the term proportional to Re is now stabilizing and the term proportional to cot θ is destabilizing. This result is consistent with previous studies[11,13,14] for flow down a rigid incline ($\Gamma\to0$). The term proportional to ΓH is now destabilizing for the LL mode. In $c_{gl}^{(1)}$ and $c_{ll}^{(1)}$ [Eqs. (29) and (31)], the relative contributions of different terms are such that it is not possible to simultaneously stabilize both the interfaces. For example, if $\mu_r=2$, $\beta=0.5$, $\theta=\pi/2$ then $(\Gamma H)<0.0147$ Re for LL mode to remain stable while $(\Gamma H)>0.106$ Re for stabilizing the GL mode low-k perturbations. Hence, it is not possible to stabilize long-wave perturbations for $\mu_r>1$. However, these results indicate that it may be possible to selectively destabilize the LL interface and this may be exploited in microfluidic applications involving the formation of uniformly sized drops via the interfacial instability. We have verified that the qualitative features of above results hold for any value of $\mu_r>1$ and is independent of β, and the results are summarized in Tables III and IV in the Appendix.

B. Mode identification

A comparison of eigenvalues obtained from zero Reynolds number analysis and low wave-number asymptotic analysis is used to identify GL, LL, and LS interfacial modes. The characteristic equation is quartic in complex wave-speed c at Re=0. The four roots of the characteristic equation are obtained using the symbolic package MATHEMATICA, once we specify k, H, Γ, θ, Σ, Σ_1 and Σ_2. The two leading order wave-speeds, $c_{gl}^{(0)}$ and $c_{ll}^{(0)}$, obtained from the low-k asymptotic analysis for flow past deformable solid are equal to the leading order wave-speeds for GL and LL modes obtained by Kao[11] for a rigid incline. In the presence of deformable solid, at Re=0, but for $k\ll1$, the real part of one of the four roots approaches the leading order wave-speed $c_{gl}^{(0)}$ of low-k asymptotic solution. This root is identified as the GL mode. Similarly, among the remaining three roots, one root approaches the leading order wave-speed $c_{ll}^{(0)}$ of the low-k asymptotic solution for $k\ll1$. This root is identified as the LL mode. Out of the remaining two roots obtained from the Re=0 analysis, one root is highly stable at low-k becomes unstable at high k when Γ increases beyond a critical value. This behavior is typical of unstable mode predicted first by Gkanis and Kumar[31] for flow past a neo-Hookean elastic solid. This root is designated as LS mode in the present study. The fourth root was never observed to have a positive growth rate for a wide range of

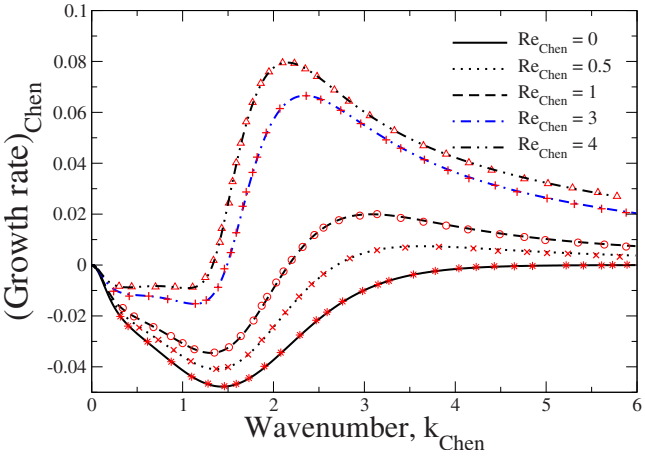

FIG. 2. (Color online) Validation of our numerical procedure by comparison with results of Ref. 14: Growth rate vs wavenumber curve for interfacial mode at different values of Reynolds number for the parameters corresponding to Fig. 13 of Ref. 14. The continuous lines represent data obtained from our numerical code by setting Γ or $H\to 0$ and the various symbols represent digitally scanned data from Fig. 13 of Ref. 14. Data for $\mu_r=0.4$, $\beta=0.5$, $\Sigma=0$, $\Sigma_1=0$, and $\theta=0.2$.

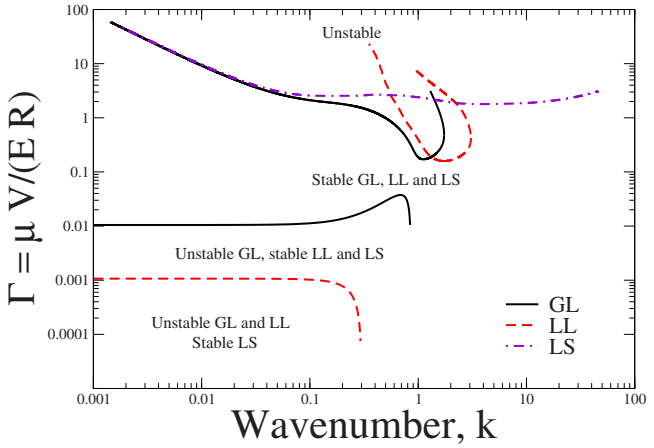

FIG. 3. (Color online) Neutral stability diagram: Γ vs k for $\mu_r=0.5$, $\beta=0.5$, $\theta=90°$, $H=2$, Re=0.1, $\Sigma=\Sigma_1=\Sigma_2=0.1$, and $\eta_r=0$.

parameters. Once identified in the above manner, each of these interfacial modes is then continued to arbitrary Re and k. A numerical shooting procedure is used to continue results at Re=0 to finite Re. Further, at finite Reynolds number, the characteristic equation is transcendental and admits multiple solutions to c unlike the zero Re limit. (We discuss the identification and labeling of such unstable modes a little later.) Thus, we also used a Chebyshev–Tau spectral method[40,41] which does not require any initial guess and resolves the entire eigenspectrum of the problem. By way of benchmarking our numerical procedures, we have made extensive comparisons of the results obtained from our codes in the limit of a rigid solid layer ($\Gamma\to 0$ and $H\to 0$) for which results are reported in the earlier papers of Chen[14] and Jiang *et al.*[15] In Fig. 2, we show one such comparison with Fig. 13 of Ref. 14, which demonstrates the correctness of our numerical code.

C. Numerical results

As discussed in Sec. I, for a rigid incline, when $\mu_r<1$, both interfaces can become unstable above a critical Reynolds number (which is zero when $\theta=\pi/2$), while for $\mu_r>1$, it is not possible to simultaneously stabilize both the modes at any Reynolds number. Hence, in the following subsections, we discuss the cases of $\mu_r<1$ and $\mu_r>1$ separately.

1. More viscous liquid adjacent to deformable wall ($\mu_r<1$)

It was shown in Sec. III A that both GL and LL modes can be stabilized for $k\ll 1$ when Γ increases beyond a critical value. From earlier works, it is also known that the solid layer deformability has a destabilizing effect on gas-liquid free surface[28] and liquid-liquid interfacial mode[25] for finite-k perturbations when solid becomes sufficiently deformable. Further, as discussed in Sec. III B, for flow past neo-Hookean elastic solid, high-wavenumber perturbations become unstable even in creeping-flow limit when $\Gamma\sim O(1)$ and increases beyond a critical value.[31,42,30,28] Since short-wave perturbations are confined to the fluid-solid interface, we expect a similar short-wave instability to exist for the present configuration as well. Moreover, Gkanis and Kumar[42] and Gaurav and Shankar[28] have shown, respectively, for Poiseuille flow in a neo-Hookean deformable channel and gravity-driven flow of single liquid film past a neo-Hookean surface that the LS interface becomes unstable for finite wavenumber perturbations with increase in solid deformability.

For the present configuration, our numerical results show that when Γ is sufficiently high, the LS mode becomes unstable for high-wavenumber perturbations even for Re=0. However, the LS mode does not become unstable at finite k for any value of Γ at Re=0. This result is at variance with the earlier predictions of Gkanis and Kumar[42] and Gaurav and Shankar,[28] and is a consequence of implementing modified stress continuity conditions in this study wherein Taylor-expansion is not carried out for Lagrangian variables in the solid layer.[38] Thus, while stabilization of GL and LL modes is achieved for long wavelength perturbations when Γ increases beyond a particular value, with further increase in Γ, all three interfaces can become unstable. Consequently, it is necessary to examine whether the suppression of low-k perturbations extends to finite-k as well. In addition, will there be a sufficient window in the parameter Γ where stable flow configuration can be achieved, i.e., all three interfaces remain stable? We first present the results for flow down a vertical plane ($\theta=\pi/2$) and when the thicknesses of two liquid layers are equal ($\beta=0.5$). We fix $\mu_r=0.5$ for discussing the results for $\mu_r<1$.

We present the results in terms of neutral stability diagrams in $\Gamma-k$ plane, which distinguish stable and unstable regions for the present three-layer system. Figure 3 shows the neutral stability diagram in $\Gamma-k$ plane for Re=0.1 and $H=2$ for all the three interfacial modes. For $\Gamma=0$ (rigid-wall limit), both GL and LL interfaces are unstable. As Γ is increased beyond the lower LL mode neutral curve, the LL interface becomes stable for perturbations of arbitrary wavelengths. The GL interface still remains unstable for perturba-

tions with wavenumbers up to 0.8. The LS interface remains stable for lower values of Γ. With further increase in Γ above the lower GL mode neutral curve, there is a transition from unstable to stable perturbations of the GL mode. When Γ is further increased, we encounter a set of three neutral curves corresponding to GL, LL, and LS modes. When Γ is increased above a particular neutral curve, the corresponding interface becomes unstable due to the deformability of solid layer. Importantly, there exists a region in Γ between the lower GL mode neutral curve and upper GL or LL neutral curves, where both GL and LL interfaces are stabilized due to the deformability of solid layer without destabilizing the LS interface. Thus, this figure shows that it is possible to achieve a stable flow configuration by appropriately selecting the solid deformability parameter Γ. To ensure that there are no unstable modes in the stable region shown in Fig. 3, we used a spectral code to verify that all eigenvalues remain stable within the stable gap of Fig. 3. Another feature worth noting in Fig. 3 is the gap between the lower LL and GL mode neutral curves. For values of Γ between the lower LL and GL mode neutral curves, the GL interface remains unstable while the LL interface is stabilized due to solid deformability. Thus, it is possible to selectively destabilize the GL mode while keeping all the other modes stable. The growth rate and wavelength of the perturbations in the system would then correspond to those for the GL mode. This feature can be potentially employed in pattern formation applications, wherein patterns of a particular wavelength can be "transferred" across all the three layers. This could also be potentially exploited in microfluidic devices that are used to form drops or particles of desired size. The drops are formed by an instability of the interface, which can be manipulated selectively by changing the deformability of the wall.

Figure 3 shows that for low-wavenumbers, there is a transition from stable to unstable perturbations when Γ is increased beyond the upper GL mode neutral curve. This is at variance with the low-k asymptotic results, where the solid layer contribution for GL mode (term proportional to ΓH) in Eq. (25) occurs with negative sign (Sec. III A). The reason for this difference is that in the long-wave asymptotic analysis, we have assumed that $\Gamma \sim O(1)$ and $c \sim O(1)$. However, for the upper GL mode neutral curve in Fig. 3, our numerical results show that $\Gamma \propto 1/k$ and $c_r \propto 1/k^{0.5}$ for $k \ll 1$. We find that the continuation of the LS mode to low k also shows a similar scaling behavior for Γ and c_r for $k \ll 1$. The low-k solution and upper GL mode neutral curve (for low-wavenumbers) represent two different classes of solutions of the eigenvalue problem depending on the scaling of Γ and c with k.

We further find that for a fixed k, $\Gamma \propto 1/\mathrm{Re}$ for $\mathrm{Re} \ll 1$ for neutral modes. This scaling implies that $\rho V^2/E \sim 1$, indicating a balance of inertial stresses and elastic stresses in the limit of low Re. Such modes are therefore dependent on the presence of inertia in the fluid and solid, and hence are a class of "inertial" LS modes,[43,45,46] which are absent at Re=0. As demonstrated below for the high-k instability, this GL mode instability, in fact, merges with one of the inertial modes described in Refs. 44–46. It is observed that the short-wave LS mode (discussed above in Sec. III B) also continues

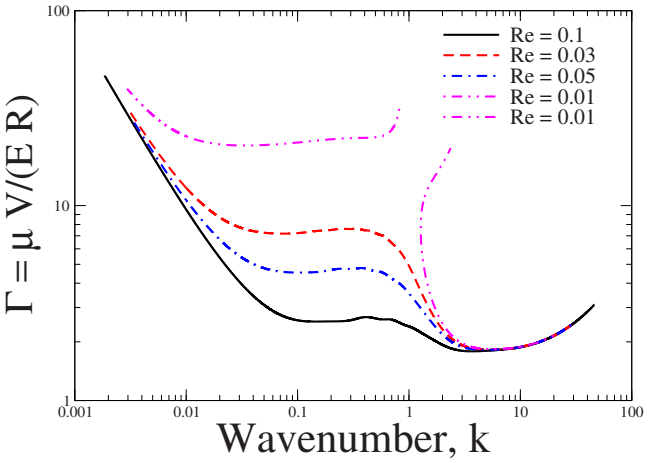

FIG. 4. (Color online) Merging of neutral curves at finite Re. Data for $\mu_r=0.5$, $\beta=0.5$, $\theta=90°$, $H=2$, $\Sigma=\Sigma_1=\Sigma_2=0.1$, and $\eta_r=0$.

to low k for finite Reynolds number (see Fig. 3). It shows identical scaling behavior for Γ with k (for $k \ll 1$) and Re (for $\mathrm{Re} \ll 1$) as illustrated by inertial LS mode (or the extended GL mode upper neutral curve in Fig. 3). This is illustrated in Fig. 4 which shows the neutral curves for the two types of LS modes for different values of Reynolds number. For Re=0.01, there exist two distinct neutral curves: a short-wave LS mode which exists for high-wavenumbers and the second neutral curve corresponds to the inertial LS mode which exists for low and finite wavenumbers. As Re is increased, these two neutral curves merge with each other even at values as low as $\mathrm{Re} \simeq 0.03$. There exist more neutral curves corresponding to other inertial LS modes at sufficiently higher values of Γ, however, we focus our attention only on those unstable modes which determine the stability window for $\mu_r < 1$. Because of mode merging phenomena at higher values of Γ, the designation of modes as GL, LS, or inertial LS depends on the characteristic asymptotic behavior used to label a mode. The labeling of modes as GL, LL, or LS is only for ease of discussion and all that is important from a practical point of view is that it is not possible to attain stable flow configuration above sufficiently higher values of Γ. In this work, we use low-k asymptotic behavior [$\Gamma \sim O(1)$ and $c \sim O(1)$; refer Sec. III B] to label GL and LL modes while LS mode is labeled using high-k behavior in the creeping-flow limit. We find that the GL, LL, and LS modes (based on the adopted nomenclature) are the only modes which are relevant for determining the stable gap for $\mu_r < 1$. We further find that increasing the surface tension has stabilizing effect (data not shown) on each of the three upper neutral curves. The size of the unstable region for LL mode also decreases significantly with increase in surface tension parameter.

Figures 5(a) and 5(b) depict the neutral stability diagram for two different values of solid layer thickness. As evident from the low-k results (refer Sec. III A), the critical Γ required for stabilization of LL and GL interfaces increases with decrease in solid thickness. However, decreasing solid thickness has stabilizing effect on upper neutral curves. For example, while the upper LL mode neutral curve is present

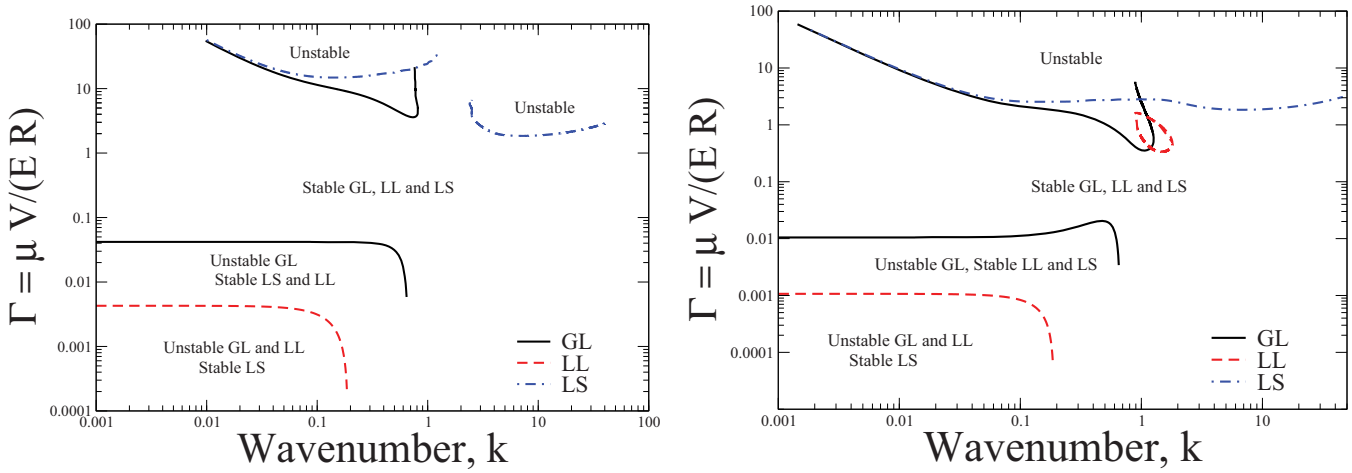

(a) $H = 0.5$ (b) $H = 2$

FIG. 5. (Color online) Effect of solid layer thickness. Data for Re=0.1, μ_r=0.5, θ=90°, Σ=Σ_1=0.25, Σ_2=0.1, and η_r=0.

for H=2, it vanishes for sufficiently thin solids [see Fig. 5(a) for H=0.5]. The critical Γ above which the GL mode is destabilized increases sufficiently when solid thickness is decreased from H=2 to H=0.5. As a result, the stable region for H=0.5 is determined by lower GL and upper LS mode neutral curves, while (in contrast) for H=2 the stable region is determined by lower and upper GL mode neutral curves. Figure 5 clearly illustrates that there is a wider region in Γ [from $\Gamma \sim O(0.01)$ to $\Gamma \sim O(1)$] for H=0.5 as compared for H=2 [from $\Gamma \sim O(0.01)$ to $\Gamma \sim O(0.1)$] where all three interfaces remain stable. The results presented thus far pertain to the case when the thickness of two liquid layers are equal, i.e., β=0.5. Figures 6(a) and 6(b) show the neutral stability diagram for two cases: when the upper less viscous liquid occupies less space (β=0.3) and when upper liquid occupies more space (β=0.7). The neutral curves for these two cases are qualitatively similar to the case when β=0.5; however, increasing β to 0.7 significantly decreases the width of stability window where all three modes can be simultaneously stabilized. On the other hand, the gap between lower GL and LL mode neutral curves, where selective stabilization of LL mode is achieved, increases with increase in β.

For $\theta = \pi/2$, the critical Reynolds number required for destabilization of GL and LL interfaces is zero for a rigid incline. However, for a nonvertical incline ($\theta \neq \pi/2$), the critical Reynolds numbers for GL and LL modes are nonzero and their values depend on fluid thickness ratio β. For example, for $\theta = \pi/4$ and β=0.5, the critical Re for GL mode is approximately 0.8 while the critical Re for LL mode is 7.79. Figure 7 shows the neutral stability diagram for H=2, $\theta = \pi/4$, β=0.5, and Re=1. The lower LL mode neutral curve is absent because the LL mode instability is not present in the first place for flow down a rigid inclined plane at Re=1. The GL interface is unstable in the rigid limit ($\Gamma \to 0$) for Re=1. As Γ is increased beyond the lower GL mode neutral curve, there is a transition from unstable to stable perturbations and a wide gap in terms of parameter Γ exists where all the modes remain stable. With further in-

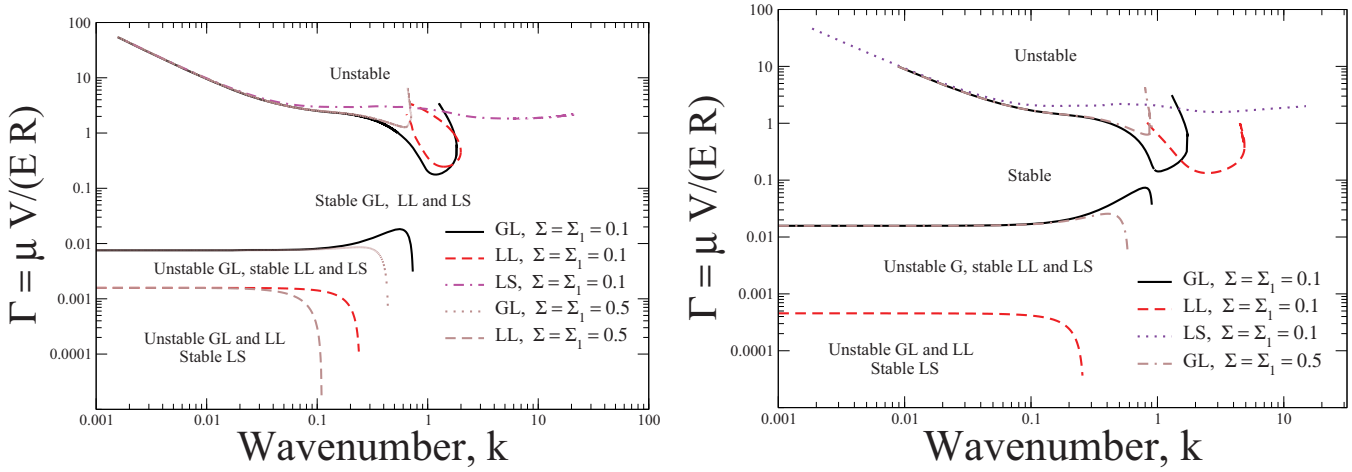

(a) $\beta = 0.3$ (b) $\beta = 0.7$

FIG. 6. (Color online) Effect of liquid layer thickness. Data for Re=0.1, μ_r=0.5, θ=90°, H=2, Σ_2=0.1, and η_r=0.

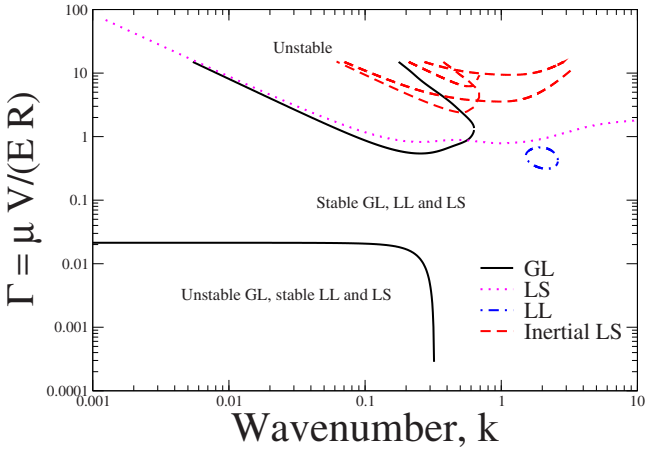

FIG. 7. (Color online) Neutral stability diagram: Γ vs k for μ_r=0.5, β =0.5, θ=45°, H=2, Re=1, Σ=Σ_1=Σ_2=0.1, and η_r=0.

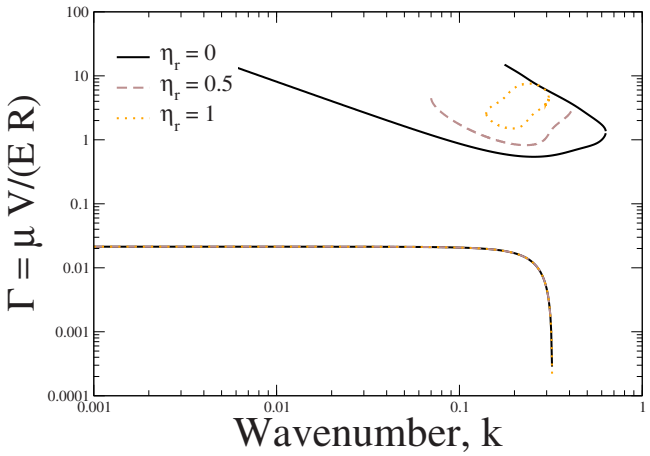

FIG. 9. (Color online) Effect of η_r on GL mode neutral stability diagram: Γ vs k data for μ_r=0.5, β=0.5, θ=45°, H=2, Re=1, Σ=Σ_1=Σ_2=0.1.

crease in Γ, the GL, LL, and LS modes become unstable (although the LL interface was stable in the rigid-wall limit). As for $\theta=\pi/2$ (Fig. 3), the GL and LS short-wave modes merge with inertial LS modes at finite Re for $\theta=\pi/4$ as well. Figure 7 also shows several other inertial LS mode neutral curves which become unstable for higher values of Γ. For Γ values within the stability window, only GL mode perturbations are being suppressed by solid layer deformability unlike the vertical flow configuration where both GL and LL modes are stabilized due to wall deformability. For $\mathrm{Re}\sim O(10)$, the low-k perturbations for both GL and LL modes can still be suppressed when Γ increases beyond a critical value. However, for such Γ, finite wavenumber modes are destabilized. Thus, a stable flow configuration cannot be achieved at Reynolds number of $O(10)$ or higher.

We next examine the effect of solid viscosity η_r. For $k \ll 1$,[27,29] the solid viscosity remains subdominant and hence does not affect the stabilization of GL or LL modes at low-wavenumbers. In Figs. 8 and 9, we examine the effect of increasing η_r on neutral stability curves presented in Fig. 7.

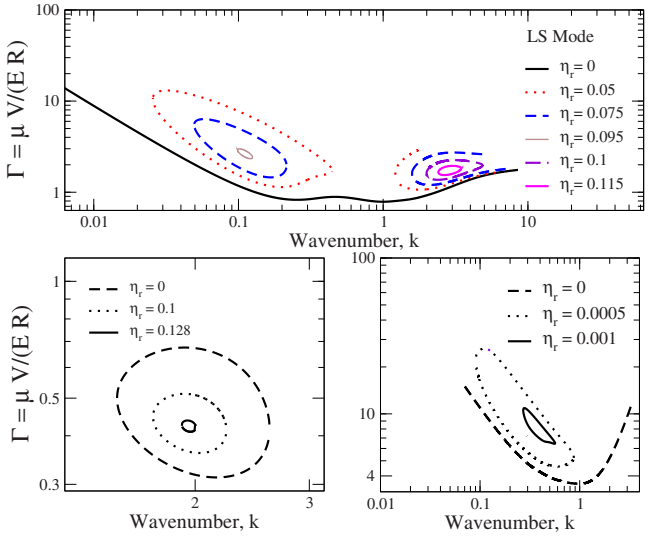

FIG. 8. (Color online) Effect of η_r on neutral stability diagram: Γ vs k for μ_r=0.5, β=0.5, θ=45°, H=2, Re=1, Σ=Σ_1=Σ_2=0.1.

Figure 8 shows that the LS neutral curve, which remains a single continuous curve for η_r=0, splits into two branches at η_r values as low as 0.05. One of the branches which exists at relatively low but finite wavenumbers corresponds to the inertial LS mode while the second branch corresponds to the short-wave LS mode. With further increase in η_r, the two branches form unstable "islands" and size of the unstable regions vanish above a critical η_r. The solid-fluid viscosity ratio also has strong stabilizing effect on LL and other inertial LS modes (which exist at relatively higher values of Γ in Fig. 7, which cease to exist beyond a critical η_r). Figure 9 shows that increasing η_r has virtually no effect on the lower neutral curve, but has stabilizing effect on upper GL mode neutral curve. However, the stabilizing effect of η_r is more prominent on upper LL and LS mode neutral curves: while the upper GL mode neutral curve exists for η_r as high as 1 (see Fig. 9), the neutral curves for LL and LS modes vanish for $\eta_r \gtrapprox 0.13$ and $\eta_r \gtrapprox 0.001$ (see Fig. 8), respectively. Thus, for η_r above a critical value, the width of stability window is determined by lower and upper GL mode neutral curves. Figure 9 illustrates that the size of the stable region (in terms of parameter Γ) increases with increase in η_r for β=0.5. A survey of our other results (data not displayed here) for nonzero solid-fluid viscosity ratio shows that increasing dissipation in solid can be used to increase the width of stability window for $\beta \leq 0.5$. For $\beta \sim 0.6$ and larger, the area of the LL mode neutral curve decreases with increase in η_r, however, the stabilization for $\beta \geq 0.6$ is not strong enough as compared to β=0.5 (Fig. 8).

It is useful at this point to provide some estimates for the dimensional parameters in the system for which the predicted suppression of instability may be observed in experiments. The Reynolds number Re based on the lower fluid viscosity is proportional to $\rho^2 g R^3/\mu_b^2$ and the solid deformability parameter $\Gamma \propto \rho g R/E$. Figure 5 shows that for μ_r=0.5, Re=0.1, η_r=0, and $\theta=\pi/2$, $\Gamma > 0.01$ for suppression of both the GL and LL interfacial instabilities. If we consider $R \sim 10^{-3}$ m, $\rho \sim 10^3$ kg/m^3, then the shear modulus $E \sim 10^3$ Pa in order for $\Gamma > 0.01$. For $\mathrm{Re} \sim 0.1$, we require $\mu_b \sim 0.3$ Pa s and $\mu_a \sim 0.15$ Pa s. Thus, the predicted

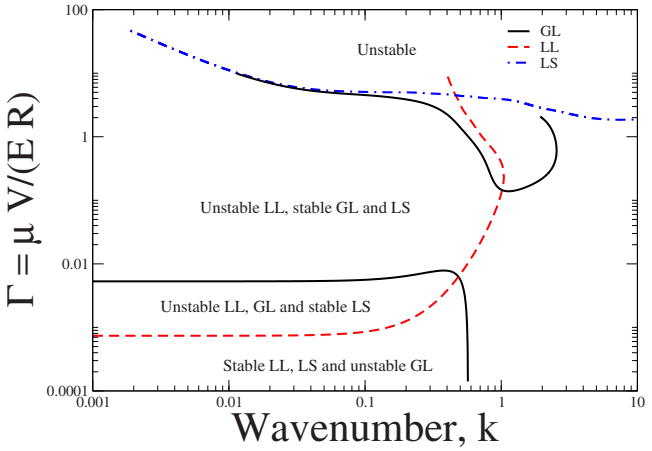

FIG. 10. (Color online) Neutral stability diagram: Γ vs k for $\mu_r=2$, $\beta=0.5$, $\theta=90°$, $H=2$, Re=0.1, $\Sigma=\Sigma_1=\Sigma_2=0.1$, and $\eta_r=0$.

suppression of instability of two-layer flows can be realized in systems involving very viscous liquids flowing past highly deformable soft solid materials.

2. Less viscous liquid adjacent to deformable wall ($\mu_r>1$)

For $\mu_r>1$, the long-wave results (Table III) show that in the low-k limit, the solid layer has a stabilizing effect on the GL mode and destabilizing effect on the LL mode. Figure 10 shows the neutral stability diagram for $\theta=\pi/2$, $\mu_r=2$, $\beta=0.5$, Re=0.1, $H=2$, $\Sigma=\Sigma_1=0.1$, $\Sigma_2=0.1$, and $\eta_r=0$. In the rigid-wall limit ($\Gamma\to 0$), the LL mode remains stable while GL mode is unstable due to inertia. As Γ is increased above the LL mode neutral curve, the LL interface is destabilized by the deformability of solid layer. With further increase in Γ, the GL mode fluctuations are suppressed by deformable coating. Thus, for Γ values above lower GL mode neutral curve, the GL and LS interfaces remain stable, while LL interface can be selectively destabilized by the soft solid layer. On further increasing Γ, we encounter upper neutral curves for GL and LS modes above which the corresponding mode becomes unstable. The LL mode neutral curve is now a single continuous curve with wavenumbers lying above and left of the neutral curve being unstable. For $\mu_r=2$, there is no region in $\Gamma-k$ plane where all the modes are stable for all wavenumbers. However, for $k<1$, there is a wide region in Γ where the LL mode can be preferentially destabilized while all other modes remain stable.

TABLE I. LL mode results from long-wave analysis for $\mu_r=0.5$ at different values of β.

β	$c_{ll}^{(0)}$	$c_{ll}^{(1)}$
0.1	1.005 98	$i(1.38\times10^{-4}\ \mathrm{Re}-6.80\times10^{-4}\ \cot\theta-4.08\times10^{-3}\Gamma H)$
0.2	1.007 75	$i(1.078\times10^{-3}\ \mathrm{Re}-5.328\times10^{-3}\ \cot\theta-3.197\times10^{-2}\Gamma H)$
0.3	0.983 729	$i(2.894\times10^{-3}\ \mathrm{Re}-1.527\times10^{-2}\ \cot\theta-9.161\times10^{-2}\Gamma H)$
0.4	0.922 429	$i(4.188\times10^{-3}\ \mathrm{Re}-2.562\times10^{-2}\ \cot\theta-1.537\times10^{-1}\Gamma H)$
0.5	0.824 609	$i(3.860\times10^{-3}\ \mathrm{Re}-3.011\times10^{-2}\ \cot\theta-1.807\times10^{-1}\Gamma H)$
0.6	0.696 944	$i(2.462\times10^{-3}\ \mathrm{Re}-2.73\times10^{-2}\ \cot\theta-1.638\times10^{-1}\Gamma H)$
0.7	0.546 240	$i(1.068\times10^{-3}\ \mathrm{Re}-1.957\times10^{-2}\ \cot\theta-1.174\times10^{-1}\Gamma H)$
0.8	0.377 641	$i(2.672\times10^{-4}\ \mathrm{Re}-1.043\times10^{-2}\ \cot\theta-6.241\times10^{-2}\Gamma H)$
0.9	0.194 73	$i(2.009\times10^{-5}\ \mathrm{Re}-2.984\times10^{-3}\ \cot\theta-1.791\times10^{-2}\Gamma H)$

TABLE II. GL mode results from long-wave analysis for $\mu_r=0.5$ at different values of β.

β	$c_{gl}^{(0)}$	$c_{gl}^{(1)}$
0.1	2.004 02	$i(0.536\ \mathrm{Re}-0.665\ \cot\theta-3.999\Gamma H)$
0.2	2.032 250	$i(0.554\ \mathrm{Re}-0.666\ \cot\theta-4.00\Gamma H)$
0.3	2.106 270	$i(0.606\ \mathrm{Re}-0.669\ \cot\theta-4.016\Gamma H)$
0.4	2.237 570	$i(0.714\ \mathrm{Re}-0684\ \cot\theta-4.102\Gamma H)$
0.5	2.425 39	$i(0.904\ \mathrm{Re}-0.720\ \cot\theta-4.319\Gamma H)$
0.6	2.663 060	$i(1.206\ \mathrm{Re}-0.783\ \cot\theta-4.700\Gamma H)$
0.7	2.943 760	$i(1.653\ \mathrm{Re}-0.877\ \cot\theta-5.254\Gamma H)$
0.8	3.263 260	$i(2.283\ \mathrm{Re}-0.997\ \cot\theta-5.985\Gamma H)$
0.9	3.615 270	$i(3.139\ \mathrm{Re}-1.149\ \cot\theta-6.998\Gamma H)$

IV. CONCLUSIONS

We have examined the effect of solid layer deformability on the stability of gravity-driven flow of two superposed liquid layers down an inclined plane lined with a deformable solid layer. We have shown that it is possible to completely stabilize the GL and LL interfacial instabilities at low Reynolds number by the deformability of the wall when $\mu_r<1$. In terms of the parameter Γ (i.e., shear modulus of the solid), the width of the stability window depends on the thickness of solid layer, relative thickness of two liquid layers, interfacial tension, and solid-fluid viscosity ratio. The effect of increasing top liquid layer thickness (β) is found to reduce the width of stability window, while increasing interfacial tension parameters (Σ and Σ_1) and solid-fluid viscosity ratio (η_r) increases the stability gap. For a vertical plane, it was shown that there exists a wide range of values of Γ where all three interfaces (GL, LL, and LS) remain stable for all wavenumbers. For small to moderate angles of inclination ($\theta\simeq\pi/4$), the suppression of instability is valid only for $\mathrm{Re}\sim O(1)$. For $\theta=\pi/4$ and $\mathrm{Re}\sim O(1)$, only the GL interface becomes unstable for flow down a rigid inclined plane. Thus, the stabilization achieved is effectively due to the suppression of the free surface instability. For the other configuration, i.e., when less viscous liquid is adjacent to soft solid

TABLE III. LL mode results from long-wave analysis for $\mu_r=2.0$ at different values of β.

β	$c_{ll}^{(0)}$	$c_{ll}^{(1)}$
0.1	0.981 965	$i(-5.92\times10^{-5}\ \mathrm{Re}+3.10\times10^{-4}\ \cot\theta+1.86\times10^{-3}\Gamma H)$
0.2	0.935 024	$i(-3.54\times10^{-4}\ \mathrm{Re}+2.085\times10^{-3}\ \cot\theta+1.25\times10^{-2}\Gamma H)$
0.3	0.867 690	$i(-7.93\times10^{-4}\ \mathrm{Re}+5.52\times10^{-3}\ \cot\theta+3.31\times10^{-2}\Gamma H)$
0.4	0.785 380	$i(-1.13\times10^{-3}\ \mathrm{Re}+9.77\times10^{-3}\ \cot\theta+5.86\times10^{-2}\Gamma H)$
0.5	0.690 983	$i(-1.20\times10^{-3}\ \mathrm{Re}+1.36\times10^{-2}\ \cot\theta+8.156\times10^{-2}\Gamma H)$
0.6	0.585 380	$i(-9.87\times10^{-4}\ \mathrm{Re}+1.57\times10^{-2}\ \cot\theta+9.43\times10^{-2}\Gamma H)$
0.7	0.467 690	$i(-5.96\times10^{-4}\ \mathrm{Re}+1.50\times10^{-2}\ \cot\theta+9.03\times10^{-2}\Gamma H)$
0.8	0.335 024	$i(-2.20\times10^{-4}\ \mathrm{Re}+1.095\times10^{-2}\ \cot\theta+6.57\times10^{-2}\Gamma H)$
0.9	0.181 965	$i(-2.56\times10^{-5}\ \mathrm{Re}+4.35\times10^{-3}\ \cot\theta+2.61\times10^{-2}\Gamma H)$

TABLE IV. GL mode results from long-wave analysis for $\mu_r=2.0$ at different values of β.

β	$c_{gl}^{(0)}$	$c_{gl}^{(1)}$
0.1	1.998 04	$i(0.532\,\mathrm{Re}-0.666\cot\theta-3.998\Gamma H)$
0.2	1.984 98	$i(0.523\,\mathrm{Re}-0.666\cot\theta-3.996\Gamma H)$
0.3	1.952 31	$i(0.501\,\mathrm{Re}-0.663\cot\theta-3.979\Gamma H)$
0.4	1.894 62	$i(0.462\,\mathrm{Re}-0.655\cot\theta-3.930\Gamma H)$
0.5	1.809 02	$i(0.406\,\mathrm{Re}-0.638\cot\theta-3.831\Gamma H)$
0.6	1.694 62	$i(0.336\,\mathrm{Re}-0.610\cot\theta-3.662\Gamma H)$
0.7	1.552 31	$i(0.259\,\mathrm{Re}-0.567\cot\theta-3.404\Gamma H)$
0.8	1.384 98	$i(0.183\,\mathrm{Re}-0.507\cot\theta-3.042\Gamma H)$
0.9	1.198 04	$i(0.116\,\mathrm{Re}-0.428\cot\theta-2.568\Gamma H)$

layer ($\mu_r>1$), deformability of the wall has a destabilizing effect on LL interfacial mode. The GL mode instability can still be suppressed for perturbations of all wavelengths. However, simultaneous stabilization of both the modes is not possible when the less viscous liquid is near the soft solid layer. The predicted phenomena were shown to be relevant in the gravity-driven flow of viscous liquids (with viscosities $\sim$1 Pa s) past soft solid surfaces (with shear modulus $\sim 10^3-10^4$ Pa).

ACKNOWLEDGMENTS

Financial support for this research was received from the Department of Science and Technology, New Delhi, India, through an IRPHA grant.

APPENDIX: RESULTS FROM LONG-WAVE ASYMPTOTIC ANALYSIS

In this appendix, we present the results obtained from the long-wave analysis for both LL and GL modes in Tables I–IV.

[1] R. G. Larson, "Instabilities in viscoelastic flows," Rheol. Acta **31**, 213 (1992).
[2] H. K. Ganpule and B. Khomami, "An investigation of interfacial instabilities in the superposed channel flow of viscoelastic fluids," J. Non-Newtonian Fluid Mech. **81**, 27 (1999).
[3] S. Scotto and P. Laure, "Linear stability of three-layer Poiseuille flow for Oldroyd-B fluids," J. Non-Newtonian Fluid Mech. **83**, 71 (1999).
[4] K. Lamnawar and A. Maazouz, "Reactive functionalized multilayer polymers in a coextrusion process: Experimental and theoretical investigations of interfacial instabilities," Int. J. Mater. Form **1**, 763 (2008).
[5] S. Millet, F. Rousset, V. Botton, and H. Ben Hadid, "Stability of a non-Newtonian two-layer film flow down an inclined plane," C. R. Mec. **336**, 331 (2008).
[6] S. J. Weinstein and K. J. Ruschak, "Coating flows," Annu. Rev. Fluid Mech. **36**, 29 (2004).
[7] A. Barrero and I. G. Loscertales, "Micro- and nano particles via capillary flows," Annu. Rev. Fluid Mech. **39**, 89 (2007).
[8] T. B. Benjamin, "Wave formation in laminar flow down an inclined plane," J. Fluid Mech. **2**, 554 (1957).
[9] C.-S. Yih, "Stability of liquid flow down an inclined plane," Phys. Fluids **6**, 321 (1963).
[10] S. P. Lin, "Instability of liquid film flowing down an inclined plane," Phys. Fluids **10**, 308 (1967).
[11] T. W. Kao, "Stability of two-layer viscous stratified flow down an inclined plane," Phys. Fluids **8**, 2190 (1965).
[12] T. W. Kao, "Role of viscosity stratification in the instability of two-layer flow down an incline," J. Fluid Mech. **33**, 561 (1968).
[13] D. S. Loewenherz and C. J. Lawrence, "The effect of viscosity stratification on the stability of a free surface flow at low Reynolds number," Phys. Fluids A **1**, 1686 (1989).
[14] K. P. Chen, "Wave formation in the gravity-driven low-Reynolds number flow of two liquid films down an inclined plane," Phys. Fluids A **5**, 3038 (1993).
[15] W. Y. Jiang, B. Helenbrook, and S. P. Lin, "Inertialess instability in two-layer liquid film flow," Phys. Fluids **16**, 652 (2004).
[16] L. Brevdo, P. Laure, F. Dias, and T. J. Birdges, "Linear pulse signaling in a film flow on an inclined plane," J. Fluid Mech. **396**, 37 (1999).
[17] R. Valette, P. Laure, Y. Demay, and J.-F. Agassant, "Convective linear stability analysis of two-layer coextrusion flow for molten polymers," J. Non-Newtonian Fluid Mech. **121**, 41 (2004).
[18] J. Hu, X. Y. Yin, H. Ben Hadid, and D. Henry, "Linear temporal and spatiotemporal stability analysis of two-layer falling films with density stratification," Phys. Rev. E **77**, 026302 (2008).
[19] P. Huerre and A. Monkewitz, "Local and global instabilities in spatially developing flows," Annu. Rev. Fluid Mech. **22**, 473 (1990).
[20] K. Alba, R. E. Khayat, and R. S. Pandher, "Steady two-layer gravity-driven thin-film flow," Phys. Rev. E **77**, 056304 (2008).
[21] M. Amaouche, N. Mehidi, and N. Amatousse, "Linear stability of a two-layer film flow down an inclined channel: A second-order weighted residual approach," Phys. Fluids **19**, 084106 (2007).
[22] S. P. Lin, J. N. Chen, and D. R. Woods, "Suppression of instability in a liquid film flow," Phys. Fluids **8**, 3247 (1996).
[23] S. P. Lin and J. N. Chen, "Elimination of three-dimensional waves in a film flow," Phys. Fluids **9**, 3926 (1997).
[24] W. Y. Jiang and S. P. Lin, "Enhancement or suppression of instability in a two-layered liquid film flow," Phys. Fluids **17**, 054105 (2005).
[25] V. Shankar and L. Kumar, "Stability of two-layer Newtonian plane Couette flow past a deformable solid layer," Phys. Fluids **16**, 4426 (2004).
[26] V. Shankar, "Stability of two-layer viscoelastic plane Couette flow past a deformable wall: Implications of fluid viscosity stratification," J. Non-Newtonian Fluid Mech. **125**, 143 (2005).
[27] V. Shankar and A. K. Sahu, "Suppression of instability in liquid flow down an inclined plane by a deformable solid layer," Phys. Rev. E **73**, 016301 (2006).
[28] Gaurav and V. Shankar, "Stability of gravity-driven free-surface flow past a deformable solid at zero and finite Reynolds number," Phys. Fluids **19**, 024105 (2007).
[29] A. Jain and V. Shankar, "Instability suppression in viscoelastic film flows down an inclined plane lined with a deformable solid layer," Phys. Rev. E **76**, 046314 (2007).
[30] V. Gkanis and S. Kumar, "Instability of gravity-driven free-surface flow past a deformable elastic solid," Phys. Fluids **18**, 044103 (2006).
[31] V. Gkanis and S. Kumar, "Instability of creeping Couette flow past a neo-Hookean solid," Phys. Fluids **15**, 2864 (2003).
[32] L. E. Malvern, *Introduction to the Mechanics of a Continuous Medium* (Prentice-Hall, Englewood Cliffs, NJ, 1969).
[33] G. A. Holzapfel, *Nonlinear Solid Mechanics* (Wiley, Chichester, 2000).
[34] M. Destrade and G. Saccomandi, "Finite-amplitude inhomogeneous waves in Mooney–Rivlin viscoelastic solids," Wave Motion **40**, 251 (2004).
[35] M. A. Hayes and G. Saccomandi, "Finite amplitude waves superimposed on pseudoplanar motions for Mooney–Rivlin viscoelastic solids," Int. J. Non-Linear Mech. **37**, 1139 (2002).
[36] M. F. Beatty and Z. Zhou, "Universal motion for a class of viscoelastic materials of differential type," Continuum Mech. Thermodyn. **3**, 169 (1991).
[37] R. L. Fosdick and J. H. Yu, "Thermodynamics, stability and non-linear oscillations of viscoelastic solids—I. Differential type solids of second grade," Int. J. Non-Linear Mech. **31**, 495 (1996).
[38] Gaurav and V. Shankar, "Stability of pressure-driven flow in a deformable neo-Hookean channel," J. Fluid Mech. **659**, 318 (2010).
[39] P. Chokshi, "Studies in the stability of Newtonian and viscoelastic flows past rigid and flexible surfaces," Ph.D. thesis, Indian Institute of Science, 2007.
[40] S. A. Orszag, "Accurate solution of the Orr–Sommerfeld stability equation," J. Fluid Mech. **50**, 689 (1971).
[41] J. J. Dongarra, B. Straughan, and D. W. Walker, "Chebyshev-Tau QZ

algorithm methods for calculating spectra of hydrodynamic stability problems," Appl. Numer. Math. **22**, 399 (1996).
[42]V. Gkanis and S. Kumar, "Stability of pressure-driven creeping flows in channels lined with a nonlinear elastic solid," J. Fluid Mech. **524**, 357 (2005).
[43]Gaurav and V. Shankar, "Stability of fluid flow through deformable neo-Hookean tubes," J. Fluid Mech. **627**, 291 (2009).
[44]V. Shankar and V. Kumaran, "Asymptotic analysis of wall modes in a flexible tube revisited," Eur. Phys. J. B **19**, 607 (2001).
[45]V. Shankar and V. Kumaran, "Stability of wall modes in fluid flow past a flexible surface," Phys. Fluids **14**, 2324 (2002).
[46]P. Chokshi and V. Kumaran, "Weakly nonlinear stability analysis of flow past a neo-Hookean solid at arbitrary Reynolds number," Phys. Fluids **20**, 094109 (2008).